

Compressed Dynamic Mode Decomposition for Real-Time Object Detection

N. Benjamin Erichson
University of St Andrews

Steven L. Brunton
University of Washington

J. Nathan Kutz
University of Washington

Abstract

We introduce the method of compressive dynamic mode decomposition (cDMD) for robustly performing real-time foreground/background separation in high-definition video. The DMD method provides a regression technique for least-square fitting of video snapshots to a linear dynamical system. The method integrates two of the leading data analysis methods in use today: Fourier transforms and Principal Components. DMD modes with temporal Fourier frequencies near the origin (zero-modes) are interpreted as background (low-rank) portions of the given video frames, and the terms with Fourier frequencies bounded away from the origin are their foreground (sparse) counterparts. When combined with compression techniques, the resulting cDMD can process full HD video feeds in real-time on CPU computing platforms while still maintaining competitive video decomposition quality, quantified by F-measure, Recall and Precision. On a GPU architecture, the method is significantly faster than real-time, allowing for further video processing to improve the separation quality and/or enacting further computer vision processes such as object recognition.

Keywords: dynamic mode decomposition, compressed sensing, object detection, background subtraction, video surveillance, robust principal component analysis.

1. Introduction

One of the most fundamental computer vision objectives is to detect moving objects in a given video stream. This is especially critical for surveillance and/or target tracking applications where accurate and real-time analysis must be accomplished. At the most basic level, dynamic pixels/objects in successive video frames are considered *foreground* objects whereas static pixels/objects are considered part of the *background*. Thus the foreground can be found in a video by removing the background, a challenging task that has been of long-standing interest in the computer vision community. This task is also known as *foreground-background separation* and/or *background modeling*. One of the great challenges in this field is to perform the separation task with HD quality video streams in real-time, something that is at the edge of performance limits for state-of-the-art algorithms. We integrate two recent innovations, the dynamic mode decomposition (DMD) [1] and compressive DMD (cDMD) [2] in order to achieve the goal of video analysis in real-time for HD quality streams. The methods take advantage of dynamical systems theory and recent developments in compressive sensing and sparsity. The results are compared against several leading methods, showing remarkable performance gains in computation time.

Algorithms for performing foreground/background separation face a number of performance challenges. Competitive methods often need to be flexible enough to accommodate changes in a scene due to, for instance, illumination changes that can occur throughout the day, or location changes where the application is being implemented. Indeed, the list of deleterious effects incurred in video processing are significant and include camera jitter, camera automatic adjustments, illumination changes, dynamic backgrounds, shadows, multiple moving foreground objects, etc. To be more precise, it is extremely rare that the camera is fixed, the background is static, only a single foreground object is present, and the illumination is constant and adequate. As such, there is no single method currently available that is capable of handling all the challenges in real videos without suffering performance failures.

Given the importance of this task for video analysis, a variety of mathematical methods and algorithms have been developed over the past decade and a half in order to perform background/foreground separation. Some of the earliest techniques developed statistical, machine learning methods for the separation process [3, 4, 5, 6], including a method based upon principal component analysis (PCA) [7]. More recent innovations have centered around low-rank and sparse matrix decompositions, or robust principal component analysis (RPCA) [8, 9, 10, 11, 12, 13], a theoretical viewpoint we will build upon with the DMD methodology. Indeed, the DMD algorithm can be shown to provide an effective way to perform an RPCA [14, 15]. So although the literature on background subtraction is immense, our focus is on these later RPCA-like techniques. However, we point the reader to several recent reviews [16, 17, 18, 19, 20] and a textbook [21] which highlight many of the methods developed and their performance metrics. Further, we direct the interested reader to the Background Subtraction website [22] which provides a comprehensive list of methods and algorithms and their relative performance on canonical data sets.

1.1. Related work

One common viewpoint of this computational task that relates closely with our method, is as a matrix separation problem into *low-rank* (background) and *sparse* (foreground) components [17, 21]. This viewpoint has been advocated, for instance, by Candès et al. in the framework of *robust principal component analysis* (RPCA) [11], and it has been extended to recent subspace tracking algorithms for foreground/background separation algorithms [20, 23, 24]. Thus, given a collection of data from a video stream, the RPCA method will seek out the sparse structures (foreground objects) within the data, while simultaneously fitting the remaining entries to a low-rank basis (static background). As long as the given data is truly of this nature, in that it lies on a low-dimensional subspace and has sparse components, then the RPCA algorithm has been proven by Candès et al. [11] to perfectly separate the given data \mathbf{X} according to

$$\mathbf{X} = \mathbf{L} + \mathbf{S} \tag{1}$$

where \mathbf{L} is low-rank and \mathbf{S} is sparse.

Key to achieving such a matrix decomposition is ℓ_1 optimization. By weighting a combination of the nuclear and the ℓ_1 norms, a convenient convex optimization problem called *principal component pursuit* (PCP) was demonstrated, under suitable assumptions, to recover the low-rank and sparse components exactly of a given data-matrix (or video for our purposes). Thus

the mathematical framework that enables PCP is given by [11]

$$\min_{\mathbf{L}, \mathbf{S}} \|\mathbf{L}\|_* + \lambda \|\mathbf{S}\|_1 \quad \text{subject to } \mathbf{X} - \mathbf{L} - \mathbf{S} = 0. \quad (2)$$

where $\|\cdot\|_*$ and $\|\cdot\|_1$ are the nuclear and ℓ_1 norms respectively, and $\lambda > 0$ is an arbitrary balance parameter that is typically chosen to be $\lambda = 1/\sqrt{\max(n, m)}$; here \mathbf{X} is an $n \times m$ matrix. This RPCA technique, which has its computational costs dominated by the convex optimization procedure, was shown to be highly-competitive in comparison to the state-of-the-art computer vision procedure developed by De La Torre and Black [12] which is based upon principal component analysis [7].

The PCP concept (2) is mathematically sound and has been successful for video processing. Its biggest challenge is computational speed and efficiency, especially given the iterative nature of the optimization required. Indeed, modern efforts around PCP have focused primarily on algorithms that overcome the computational complexity of the original algorithm. For a thorough discussion of such methods, see the recent review of Bouwmans and Zahzah [20]. This review article highlights the state-of-the-art in performing RPCA separation using the PCP framework. It also gives a comprehensive review of performance on video processing tasks, from accuracy to speed. Additionally, it compares the PCP-based methods against one of the leading mixture of Gaussians background models [3, 19].

1.2. Contribution

In this manuscript, we advocate a similar matrix decomposition approach, but by using the method of *dynamic mode decomposition* (DMD) [25, 26, 27, 28] instead of RPCA [11]. This method, which essentially implements a Fourier decomposition of the video frames in time, distinguishes the stationary background from the dynamic foreground by differentiating between the near-zero modes and the remaining modes bounded away from the origin, respectively. Originally introduced in the fluid mechanics community, DMD has emerged as a powerful tool for analyzing the dynamics of nonlinear systems [25, 26, 27, 28]. In the context of fluids, DMD has gained popularity since it provides, in an *equation-free* manner, information about the dynamics of flow even if the underlying dynamics are nonlinear. It is equation-free in the sense that a typical application requires collection of a time series of experimental (or simulated) velocity field data, from which DMD modes and eigenvalues are computed. The modes are spatial fields that often identify coherent structures in the flow. The corresponding eigenvalues define growth/decay rates and oscillation frequencies for each mode. More precisely, the DMD provides a regression to the least-square fit linear dynamical system modeling the data snapshots collected [28]. Taken together, the DMD modes and eigenvalues describe the dynamics observed in the time series in terms of growth, decay, and oscillatory components; i.e. it decomposes data into Fourier modes in time [29].

In the application of video surveillance, the video frames can be thought of as snapshots of some underlying complex/nonlinear dynamics. The DMD yields oscillatory time components of the video frames that have contextual implications. Namely, those modes that have eigenvalues near the origin represent dynamics that are unchanging, or changing slowly, and can be interpreted as stationary background pixels, or low-rank components of the data matrix. In contrast, those modes bounded away from the origin are changing on $\mathcal{O}(1)$ timescales or faster, and represent the foreground motion in the video, or the sparse components of the data matrix. Thus, by simply applying the dynamical systems interpretation of DMD to

video frames, an approximate RPCA technique can be enacted at a fixed cost of a singular-value decomposition and a linear equation solve. Unlike the convex optimization procedure of Candès et al. [11], which can be guaranteed to exactly produce a low-rank and sparse separation under certain assumptions, no such guarantees are currently given for the DMD procedure. Regardless, in comparison with the RPCA [11] and computer vision [12] methods, the DMD procedure is orders of magnitude faster in computational performance since it relies on only a single singular value decomposition, resulting in real-time separation on laptop-class computing power, which suggests that this DMD technique merits serious consideration. It should be noted however, that recent advances in optimization (principal component pursuit, for instance), allows for significant improvement in computing the matrix decompositions necessary for this background separation task [17].

2. Background

2.1. Dynamic Mode Decomposition (DMD)

DMD is an *equation-free*, data-driven matrix decomposition that is capable of providing accurate reconstructions of spatio-temporal coherent structures arising in nonlinear dynamical systems, or short-time future estimates of such systems. DMD traces its origins to Bernard Koopman in 1931 [30]. However, it had limited early impact since computers had not yet been invented and only analytic results, for simple problems, could be obtained. The work of Koopman was revived by Mezić and co-workers starting in 2004 [31, 32], when both modern computers and a deep theoretical understanding of dynamical systems theory was available. In short, Koopman theory is a dynamical systems tool that provides complete information about a nonlinear dynamical system via an associated infinite-dimensional linear operator. Specifically, it provides a theoretical characterization that is readily interpretable in terms of standard methods of dynamical systems.

DMD is a special case of Koopman theory where the so-called *Koopman observables* are just the state space itself [33]. Specifically, Schmid [25] proposed the DMD architecture for modeling complex flows. The connection with Koopman theory was only made theoretically rigorous by the subsequent work of Rowley et al. [26]. The connection between the works of Mezić, Schmid and Rowley and their co-workers between 2004-2010 laid the foundations for DMD as a transformative mathematical architecture. Indeed, in the last few years alone, DMD has seen tremendous development in both theory and application. In theory, DMD has seen innovations around sparsity [34] and compressive architectures [35, 2, 36], multi-resolution analysis [37], control theory [38], robust principal components analysis (RPCA) [14, 15], and de-noising algorithms [39, 40]. In addition to continued progress in fluid dynamics, DMD has been applied to new domains, including neuroscience [41], epidemiology [42], robotics [43], and the current application of video processing and computer vision [1, 44, 14, 15].

In what follows, we use the most recent formal definition of the DMD method [27]:

Definition: Dynamic Mode Decomposition (Tu et al. 2014 [27]): *Suppose we have two*

sets of data

$$\mathbf{X} = \begin{bmatrix} | & | & & | \\ \mathbf{x}_1 & \mathbf{x}_2 & \cdots & \mathbf{x}_m \\ | & | & & | \end{bmatrix}, \quad \mathbf{X}' = \begin{bmatrix} | & | & & | \\ \mathbf{x}'_1 & \mathbf{x}'_2 & \cdots & \mathbf{x}'_m \\ | & | & & | \end{bmatrix} \quad (3)$$

where each column \mathbf{x}_k of \mathbf{X} is an initial condition and each column \mathbf{x}'_k of \mathbf{X}' is the corresponding output after some prescribed evolution time Δt with there being m initial conditions considered. The DMD modes are eigenvectors of

$$\mathbf{A} = \mathbf{X}'\mathbf{X}^\dagger \quad (4)$$

where \dagger denotes the Moore-Penrose pseudoinverse.

The definition of DMD thus yields the matrix \mathbf{A} , which is a finite dimensional approximation of the Koopman operator for a linear observable.

At its core, the DMD is a regression algorithm. Specifically, it produces a regression to the best-fit linear dynamical system for the data \mathbf{X} . The DMD procedure thus constructs the proxy, approximate linear evolution

$$\mathbf{x}_{k+1} = \mathbf{A}\mathbf{x}_k. \quad (5)$$

The eigenvalues λ_j and eigenvectors ϕ_j of \mathbf{A} characterize the system dynamics. This induces an associated continuous-time dynamical system given by

$$\frac{d\tilde{\mathbf{x}}}{dt} = \tilde{\mathbf{A}}\tilde{\mathbf{x}}, \quad (6)$$

with $\mathbf{A} = \exp(\tilde{\mathbf{A}}\Delta t)$. For an initial condition $\tilde{\mathbf{x}}(0) = \tilde{\mathbf{x}}_0$, the solution of Eq. (6) is given by

$$\tilde{\mathbf{x}}(t) = \sum_{j=1}^k b_j \phi_j \exp(\omega_j t), \quad (7)$$

where $\omega_j = \log(\lambda_j)/\Delta t$ are the continuous-time eigenvalues. The ultimate goal in the DMD algorithm is to optimally construct the matrix \mathbf{A} so that the true and approximate solutions remain optimally close in a least-square sense:

$$\|\mathbf{x}(t) - \tilde{\mathbf{x}}(t)\| \ll 1. \quad (8)$$

Of course, the optimality of the approximation holds only over the sampling window where \mathbf{A} is constructed, but the approximate solution can be used to not only make future state predictions, but also to decompose the dynamics into various time-scales since the ω_j are prescribed. Moreover, the DMD typically makes use of low-rank structure so that the total number of modes, $k \ll n$, allows for dimensionality reduction of the complex system or video stream.

In practice, when the state dimension n is large, the matrix \mathbf{A} may be intractable to analyze directly. Instead, DMD circumvents the eigendecomposition of \mathbf{A} by considering a rank-reduced representation in terms of a PCA-projected matrix $\tilde{\mathbf{A}}$. The DMD algorithm proceeds as follows [27]:

1. Compute the SVD of \mathbf{X} [45]:

$$\mathbf{X} = \mathbf{U}\mathbf{\Sigma}\mathbf{V}^*, \quad (9)$$

where $*$ denotes the conjugate transpose, $\mathbf{U} \in \mathbb{C}^{n \times k}$, $\mathbf{\Sigma} \in \mathbb{C}^{k \times k}$ and $\mathbf{V} \in \mathbb{C}^{m-1 \times k}$. Here k is the rank of the reduced SVD approximation to \mathbf{X} . The left singular vectors \mathbf{U} are essentially PCA modes.

The SVD reduction in (9) could also be exploited at this stage in the algorithm to perform a low-rank truncation of the data. Specifically, if low-dimensional structure is present in the data, the singular values of $\mathbf{\Sigma}$ will decrease sharply to zero with perhaps only a limited number of dominant modes. A principled way to truncate noisy data would be to use the recent hard-thresholding algorithm of Gavish and Donoho [46].

2. Next, compute $\tilde{\mathbf{A}}$, the $k \times k$ projection of the full matrix \mathbf{A} onto POD modes:

$$\begin{aligned} \mathbf{A} &= \mathbf{X}'\mathbf{V}\mathbf{\Sigma}^{-1}\mathbf{U}^* \\ \implies \tilde{\mathbf{A}} &= \mathbf{U}^*\mathbf{A}\mathbf{U} = \mathbf{U}^*\mathbf{X}'\mathbf{V}\mathbf{\Sigma}^{-1}. \end{aligned} \quad (10)$$

3. Compute the eigendecomposition of $\tilde{\mathbf{A}}$:

$$\tilde{\mathbf{A}}\mathbf{W} = \mathbf{W}\mathbf{\Lambda}, \quad (11)$$

where columns of \mathbf{W} are eigenvectors and $\mathbf{\Lambda}$ is a diagonal matrix containing the corresponding eigenvalues λ_j . Recall that the continuous-time eigenvalues are given by $\omega_j = \log(\lambda_j)/\Delta t$.

4. Finally, we may reconstruct eigendecomposition of \mathbf{A} from \mathbf{W} and $\mathbf{\Lambda}$. In particular, the eigenvalues of \mathbf{A} are given by $\mathbf{\Lambda}$ and the eigenvectors of \mathbf{A} (DMD modes) are given by columns of $\mathbf{\Phi}$:

$$\mathbf{\Phi} = \mathbf{X}'\mathbf{V}\mathbf{\Sigma}^{-1}\mathbf{W}. \quad (12)$$

Note that Eq. (12) from [27] differs from the formula $\mathbf{\Phi} = \mathbf{U}\mathbf{W}$ from [25], although these will tend to converge if \mathbf{X} and \mathbf{X}' have the same column spaces.

2.2. Application to Video

The DMD algorithm applies to generic, time-dependent data. Our interest in this work is to connect it to computer vision and video processing applications [1, 44, 14, 15]. For video, the data collection process involves two parameters:

$$\begin{aligned} n &= \text{number of pixels saved per time snapshot,} \\ m + 1 &= \text{number of video frames (snapshots) taken.} \end{aligned}$$

The video snapshots are arranged into two $n \times m$ matrices \mathbf{X} and \mathbf{X}' defined in the DMD algorithm.

A video sequence offers an appropriate application for DMD because the frames of the video are, by nature, equally spaced in time, and the pixel data, collected in every snapshot, can readily be vectorized. Given $m + 1$ frames of the video stream, the $n \times 1$ vectors $\mathbf{x}_1, \mathbf{x}_2, \dots, \mathbf{x}_{m+1}$ can be extracted, which contain the pixel data of each frame; there being

n pixels in total per frame. The DMD method can attempt to reconstruct any given frame, or even possibly future frames, by calculating $\mathbf{x}_{\text{DMD}}(t)$ at the corresponding time t via the DMD algorithm. The validity of the reconstruction depends on how well the specific video sequence meets the assumptions and criteria of the DMD method.

In order to reconstruct the entire video, consider the $1 \times m + 1$ time vector $\mathbf{t} = [t_1 \ t_2 \ \dots \ t_{m+1}]$, which contains the times at which the frames were collected. If $t_j = j - 1 \ \forall j$, then time becomes equivalent to the frame count, where the first frame is labelled as 0 and the last frame is labelled as m . The video sequence \mathbf{X} and \mathbf{X}' are reconstructed with the DMD approximation (7). Notice that the DMD mode ϕ_k is a $n \times 1$ vector which is used to construct an $n \times m$ video at each point of the time vector \mathbf{t} using (7). By the construction of the DMD methodology: $\mathbf{x}_1 = \Phi \mathbf{b}$, which means that $\Phi \mathbf{b}$ renders the first frame of the video with a dimensionality reduction chosen through the parameter k .

It becomes apparent that any portion of the first video frame that does not change in time, or changes very slowly in time, must have an associated eigenvalue (ω_j) that is located near the origin in complex space: $\|\omega_j\| \approx 0$. This fact becomes the key principle that makes possible the ability of the DMD method to separate background (approximate low-rank) information from foreground (approximate sparse) information.

Assume that the background mode $\omega_p \approx 0$. The DMD expansion then yields

$$\begin{aligned} \mathbf{X}_{\text{DMD}} &= \mathbf{L} + \mathbf{S} \\ &= \underbrace{b_p \phi_p \exp(\omega_p t)}_{\text{Background Video}} + \underbrace{\sum_{j \neq p} b_j \phi_j \exp(\omega_j t)}_{\text{Foreground Video}} \end{aligned} \quad (13)$$

Assuming that $\mathbf{X} \in \mathbb{R}^{n \times m}$, then a proper DMD reconstruction should also produce $\mathbf{X}_{\text{DMD}} \in \mathbb{R}^{n \times m}$. However, each term of the DMD reconstruction is complex: $b_j \phi_j \exp(\omega_j t) \in \mathbb{C}^{n \times m} \ \forall j$, though they sum to a real-valued matrix. This poses a problem when separating the DMD terms into approximate low-rank and sparse reconstructions because real-valued outputs are desired and knowing how to handle the complex elements can make a significant difference in the accuracy of the results.

We can interpret these DMD results as follows: stationary background objects translate into highly correlated pixel regions from one frame to the next, which suggests a low-rank structure within the video data. Thus the DMD algorithm can be thought of as an RPCA method [14, 15]. Specifically, DMD provides a matrix decomposition of the form $\mathbf{X} = \mathbf{L} + \mathbf{S}$, where the low-rank matrix \mathbf{L} will render the video of just the background (\mathbf{L} is the first term in (13), and the sparse matrix \mathbf{S} will render the complementary video of the moving foreground objects (\mathbf{S} is the second term in (13)). Because the foreground objects exhibit a spatial coherency throughout the video, the RPCA method is no longer guaranteed a high probability of success; however, in practice, RPCA achieves an acceptable separation almost every time. The advantage of the DMD method and its sparse/low-rank separation is the computational efficiency of achieving (13), especially when compared to the optimization methods of RPCA.

2.3. Compressed Sensing

The DMD architecture has already been demonstrated to be effective and fast in separating foreground and background objects in video [1, 44, 14, 15]. DMD has also been shown to

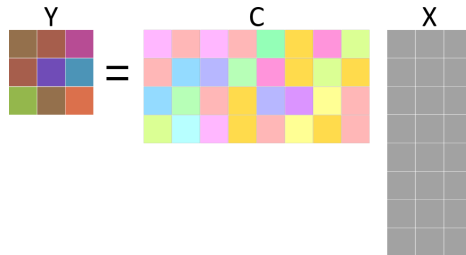


Figure 1: Compressed sensing measurement process.

be effective when using a compression architecture [2]. Our goal is to combine these two methods to provide a transformationally fast algorithm for video processing and computer vision applications. Indeed, compression algorithms are at the core of modern video, image and audio processing software such as MPEG, JPEG and MP3.

In our mathematical infrastructure of cDMD, we consider the theory of compressed sensing as developed from 2006 onwards [47, 48, 49, 50, 51, 52]. It demonstrates that instead of measuring the high-dimensional signal, or pixel space representation of a single frame \mathbf{x} , we can measure instead a low-dimensional subsample \mathbf{y} and approximate/reconstruct the full state space \mathbf{x} with this significantly smaller measurement. Specifically, compressive sensing assumes the data being measured is compressible in some basis, which is certainly the case for video. Thus the video can be represented in a small number of elements of that basis, i.e. we only need to solve for the few non-zero coefficients in the transform basis. For instance, consider the measurements $\mathbf{y} \in \mathbb{R}^p$, with $k < p \ll n$:

$$\mathbf{y} = \mathbf{C}\mathbf{x},$$

as shown in Fig. 1. The measurement matrix \mathbf{C} is often denoted by Φ in the compressed sensing literature. However, Φ is already used to represent DMD modes.

If \mathbf{x} is sparse in Ψ , then we may solve the underdetermined system of equations

$$\mathbf{y} = \mathbf{C}\Psi\mathbf{s} \tag{14}$$

for \mathbf{s} and then reconstruct \mathbf{x} . Since there are infinitely many solutions to this system of equations, we seek the sparsest solution $\hat{\mathbf{s}}$. However, it is well known from the compressive sensing literature that solving for the sparsest solution formally involves an ℓ_0 optimization that is NP-hard and computationally intractable. The success of compressive sensing is that it ultimately engineered a solution around this issue by showing that one can instead, under certain conditions on the measurement matrix \mathbf{C} , trade the infeasible ℓ_0 optimization for a convex ℓ_1 -minimization [50, 47]:

$$\hat{\mathbf{s}} = \underset{\mathbf{s}'}{\operatorname{argmin}} \|\mathbf{s}'\|_1, \text{ such that } \mathbf{y} = \mathbf{C}\Psi\mathbf{s}'. \tag{15}$$

Thus the ℓ_1 -norm acts as a proxy for sparsity promoting solutions of $\hat{\mathbf{s}}$.

To guarantee that the compressive sensing architecture will *almost certainly* work in a probabilistic sense, the measurement matrix \mathbf{C} and sparse basis Ψ must be *incoherent*, meaning that the rows of \mathbf{C} are uncorrelated with the columns of Ψ . Incoherence is quantified by the

function $\mu(\mathbf{C}, \Psi)$:

$$\mu(\mathbf{C}, \Psi) = \sqrt{n} \max_{i,j} |\langle \mathbf{c}_j, \psi_i \rangle|,$$

where \mathbf{c}_j is the j -th row of \mathbf{C} and ψ_i is the i -th column of Ψ .

For incoherent measurements, the matrix $\mathbf{C}\Psi$ satisfies a *restricted isometry property* (RIP), so it acts like an isometry map on sparse vectors \mathbf{s} ,

$$(1 - \delta_k) \|\mathbf{s}\|_2^2 \leq \|\mathbf{C}\Psi\mathbf{s}\|_2^2 \leq (1 + \delta_k) \|\mathbf{s}\|_2^2, \quad (16)$$

where δ_k is the restricted isometry constant [53]. This constant δ_k is the smallest number that satisfies Eq. (16) for *all* k -sparse vectors \mathbf{s} . For small δ_k , the map $\mathbf{C}\Psi$ acts as a near isometry on k -sparse vectors \mathbf{s} , so that distances and angles are preserved between sparse vectors. It is difficult to compute δ_k directly, and we generally prefer a statistical description of the bounds on δ_k since \mathbf{C} will be randomly generated. Typically, increasing the number of measurements will decrease the restricted isometry constant δ_k , thus making $\mathbf{C}\Psi$ closer to an isometry on sparse vectors. On the order of $k \log(n/k)$ measurements must be acquired for a δ_k that enables exact reconstruction of the k nonzero elements of the n -length vector \mathbf{s} for noiseless data [54, 48, 51]. An in-depth discussion of incoherence and the RIP can be found in [51, 53]. The restricted isometry property of $\mathbf{C}\Psi$ will facilitate compressed dynamic mode decomposition for data with low-rank structure.

Given that we are considering video images, it is easy to suggest the use of generic basis functions such as Fourier or wavelets in order to represent the sparse signal \mathbf{s} . Indeed, wavelets are already the standard for image compression architectures such as JPEG-2000. As for the Fourier transform basis, it is particularly attractive for many engineering purposes since single-pixel measurements are clearly incoherent given that it excites broadband frequency content. If an image is k -sparse in the Fourier domain, we may then reconstruct the full image from $\mathcal{O}(k \log(n/k))$ single-pixel measurements at random spatial locations. In addition to Fourier and wavelet basis functions, compressive sensing has shown that Bernoulli and Gaussian random measurement matrices \mathbf{C} satisfy the RIP property with high probability for a generic basis Ψ [49]. There is also work describing incoherence with sparse matrices and generalizations to the RIP [55]. More optimally, one can pair the compressive sensing scheme with a data-driven POD/PCA basis, in which the data is optimally (in an ℓ_2 -sense) sparse [28, 56, 57, 58, 59]. The use of a POD/PCA basis results in a more computationally efficient signal reconstruction from even fewer measurements.

More generally, there have been a significant number of innovations around sparsity and sparse representation using ℓ_1 minimization and/or *greedy algorithms* [60, 61, 62, 63] that iteratively determine sparse solutions to the underdetermined system in Eq. (14). The compression ideology is also critical for producing efficient algorithms associated with compressed SVD and PCA computations based on the Johnson-Lindenstrauss (JL) lemma [64, 65, 66, 63]. The JL lemma is closely related to the RIP, and it states when it is possible to embed a set of high-dimensional vectors in a low-dimensional space while preserving the spectral properties.

3. Compressed DMD (cDMD)

Compressed DMD provides a computationally efficient framework to compute the dynamic mode decomposition on massively under-sampled or compressed data [2]. The method was

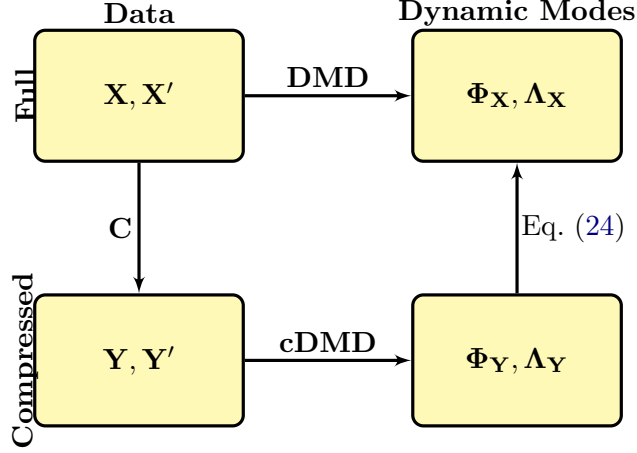


Figure 2: Schematic illustrating the compressed DMD architecture. Full data is first compressed via left multiplication by a compression matrix \mathbf{C} . Next, DMD is performed on the compressed data. Finally, full DMD modes $\Phi_{\mathbf{X}}$ may be reconstructed from compressed modes $\Phi_{\mathbf{Y}}$ by the expression in Eq. (24).

originally devised to reconstruct high-dimensional, full-resolution DMD modes from sparse, spatially under-resolved measurements by leveraging compressed sensing. However, it was quickly realized that if full-state measurements are available, many of the computationally expensive steps in DMD may be computed on a compressed representation of the data, providing dramatic computational savings. The first approach, where DMD is computed on sparse measurements without access to full data, is referred to as *compressed sensing DMD* (csDMD). The second approach, where DMD is accelerated using a combination of calculations on compressed data and full data, is referred to as *compressed DMD* (cDMD); this is depicted schematically in Fig. 2. For the applications explored in this work, we use the compressed DMD, since full image data is available and reducing algorithm run-time is critical for real-time performance.

3.1. Algorithm

For both compressed DMD (cDMD) and compressed sensing DMD (csDMD), we consider compressed measurements \mathbf{y} that are related to the full image \mathbf{x} by:

$$\mathbf{y} = \mathbf{C}\mathbf{x}. \quad (17)$$

Again, the matrix $\mathbf{C} \in \mathbb{R}^{p \times n}$ compresses or sub-samples the data in \mathbf{x} . These compressed measurements are stacked as the columns of data matrices as in Eq. (3):

$$\mathbf{Y} = \mathbf{C}\mathbf{X}, \quad \mathbf{Y}' = \mathbf{C}\mathbf{X}'. \quad (18)$$

There is a fundamental assumption that each of the columns of \mathbf{X} and \mathbf{X}' are sparse in some transform basis Ψ , so that $\mathbf{X} = \Psi\mathbf{S}$ and $\mathbf{X}' = \Psi\mathbf{S}'$. Thus, for sufficiently many incoherent measurements, the compressed matrices \mathbf{Y} and \mathbf{Y}' have similar correlation structures to

their high-dimensional counterparts, as in the compressed sensing discussion above. This is discussed in more detail in [2].

The compressed DMD algorithm proceeds similarly to full-state DMD at nearly every step until the computation of the DMD modes. Compressed DMD approximates the eigenvalues and eigenvectors of the linear map \mathbf{A}_Y defined as:

$$\mathbf{A}_Y = \mathbf{Y}'\mathbf{Y}^\dagger \quad (19a)$$

$$= \mathbf{Y}'\mathbf{V}_Y\Sigma_Y^{-1}\mathbf{U}_Y^*, \quad (19b)$$

where the pseudo-inverse \mathbf{Y}^\dagger is computed using the SVD:

$$\mathbf{Y} = \mathbf{U}_Y\Sigma_Y\mathbf{V}_Y^*. \quad (20)$$

Note that the subscript Y is included to explicitly denote computations and data obtained from the compressed data Y . As in the standard DMD algorithm, we typically do not compute the large matrix \mathbf{A}_Y , but instead compute the low-dimensional model projected onto POD/PCA modes:

$$\tilde{\mathbf{A}}_Y = \mathbf{U}_Y^*\mathbf{A}_Y\mathbf{U}_Y \quad (21a)$$

$$= \mathbf{U}_Y\mathbf{Y}'\mathbf{V}_Y\Sigma_Y^{-1}. \quad (21b)$$

The eigendecomposition of $\tilde{\mathbf{A}}_Y$ yields

$$\tilde{\mathbf{A}}_Y\mathbf{W}_Y = \mathbf{W}_Y\Lambda_Y, \quad (22)$$

and the compressed DMD modes are given by

$$\Phi_Y = \mathbf{Y}'\mathbf{V}_Y\Sigma_Y^{-1}\mathbf{W}_Y. \quad (23)$$

To obtain full-state DMD modes, we may either apply compressed sensing to each mode in Φ_Y , which would be *compressed sensing DMD*, or we may apply the linear transformations obtained using Y and Y' to the full-state data X' :

$$\tilde{\Phi}_X = \mathbf{X}'\mathbf{V}_Y\Sigma_Y^{-1}\mathbf{W}_Y. \quad (24)$$

Note that the compressed DMD modes in Eq. (24) make use of the full data X' as well as the linear transformations obtained using the compressed data Y and Y' . The expensive SVD on X is bypassed, and it is instead performed on Y . Depending on the compression ratio, this may provide significant computational savings.

The compressed DMD computation is described in Algorithm 1, and more theoretical and numerical details about the compressed DMD architecture are provided in 3. However, it is important to note that many fewer measurements may be used in compressed DMD than in compressed sensing DMD. In a variety of examples, as few as $\mathcal{O}(10) - \mathcal{O}(100)$ measurements were sufficient to yield excellent compressed DMD eigenvalues and modes. There are a few conditions on the data and compression that must be met for compressed DMD to work, but in practice these are less stringent than the requirements for compressed sensing. In addition, examples indicate that fewer compressed measurements are required to resolve low-frequency DMD modes, such as the zero-frequency background mode.

Algorithm 1 Compressed DMD (cDMD)**Input:** $\mathbf{D} \in \mathbb{R}^{n \times m}$, target rank k and sensors p .**Require:** $m \geq n$, integer $k, p \geq 1$ and $k \ll n$

```

1: procedure cDMD( $\mathbf{D}$ ,  $k$ )
2:    $\mathbf{X}, \mathbf{X}' \leftarrow \mathbf{D}$  ▷ Left/right snapshot sequence.
3:    $\mathbf{C} \leftarrow \text{rand}(p, m)$  ▷ Draw  $p \times m$  sensing matrix.
4:    $\mathbf{Y}, \mathbf{Y}' \leftarrow \mathbf{C} * \mathbf{D}$  ▷ Compress input matrix.
5:    $\mathbf{U}, \mathbf{s}, \mathbf{V} \leftarrow \text{svd}(\mathbf{Y}, k)$  ▷ Truncated SVD.
6:    $\mathbf{S} \leftarrow \text{diag}(\mathbf{s}^{-1})$  ▷ Inversed diagonal matrix.
7:    $\tilde{\mathbf{A}} \leftarrow \mathbf{U}^* * \mathbf{Y}' * \mathbf{V} * \mathbf{S}$  ▷ Least squares fit.
8:    $\mathbf{W}, l \leftarrow \text{eig}(\tilde{\mathbf{A}})$  ▷ Eigenvalue decomposition.
9:    $\mathbf{F} \leftarrow \mathbf{X}' * \mathbf{V} * \mathbf{S} * \mathbf{W}$  ▷ Compute full-state modes  $\Phi_X$ .
10:   $\mathbf{b} \leftarrow \text{lstsq}(\mathbf{F}, \mathbf{x}_1)$  ▷ Compute amplitudes.
11:   $\mathbf{V} \leftarrow \text{vander}(l)$  ▷ Vandermonde matrix.
12:  return  $\mathbf{F} \in \mathbb{C}^{n \times k}, \mathbf{b} \in \mathbb{C}^k, \mathbf{V} \in \mathbb{C}^{k \times n}$ 
13: end procedure

```

3.2. Measurement matrices

A basic sensing matrix \mathbf{C} can be constructed by drawing $p \times n$ independent random samples from a Gaussian, Uniform or a sub Gaussian, e.g., Bernoulli distribution. It can be shown that these measurement matrices have optimal theoretical properties, however for practical large-scale applications they are often not feasible. This is because generating a large number of random numbers can be expensive and computing (18) using unstructured dense matrices has a time complexity of $O(pnm)$. From a computational perspective it is favorable to build a structured random sensing matrix which is memory efficient and enables the execution of fast matrix-matrix multiplications. For instance, Woolfe et al. [67] showed that the costs can be reduced to $O(\log(p)nm)$ using a subsampled random Fourier transform (SRFT) sensing matrix

$$\mathbf{C} = \mathbf{RFD} \quad (25)$$

where $\mathbf{R} \in \mathbb{C}^{p \times n}$ draws p random rows (without replacement) from the identity matrix $\mathbf{I} \in \mathbb{C}^{n \times n}$. $\mathbf{F} \in \mathbb{C}^{n \times n}$ is the unnormalized discrete Fourier transform with the following entries $\mathbf{F}(j, k) = \exp(-2\pi i(j-1)(k-1)/m)$ and $\mathbf{D} \in \mathbb{C}^{n \times n}$ is a diagonal matrix with independent random diagonal elements uniformly distributed on the complex unit circle. While the SRFT sensing matrix comes with nice theoretical properties, the improvement from $O(k)$ to $O(\log(k))$ is not necessarily significant if the effective rank is small as in video applications. Surveillance videos are known for having a rapidly decaying spectrum, hence the required number k of dominant singular values is small. In practice it is often sufficient to construct even simpler sensing matrices to achieve similar performance. An interesting approach making the matrix-matrix multiplication (18) redundant is to use just single-pixel measurements

$$\mathbf{C} = \mathbf{R} \quad (26)$$

In a practical implementation this allows one to construct the compressed matrix \mathbf{Y} by just choosing p random rows without replacement from \mathbf{X} . Hence, only p random numbers have to be generated and no memory is required for storing a sensing matrix \mathbf{C} . A different approach

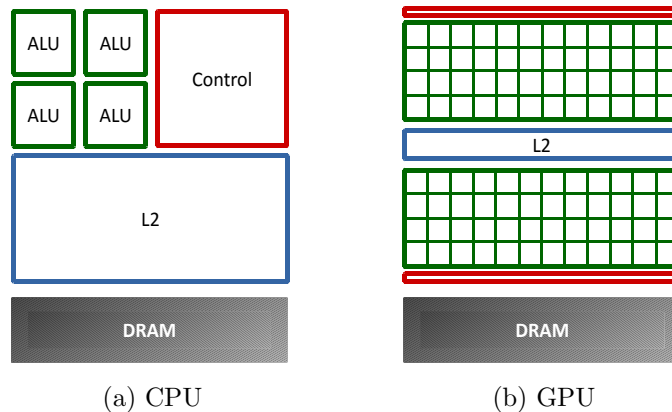


Figure 3: Illustration of the CPU and GPU architecture.

is the method of sparse random projections [68]. The idea is to construct a sensing matrix \mathbf{C} with identical independent distributed entries as follows

$$c_{ij} = \begin{cases} 1 & \text{with prob. } \frac{1}{2s} \\ 0 & \text{with prob. } 1 - \frac{1}{s} \\ -1 & \text{with prob. } \frac{1}{2s} \end{cases} \quad (27)$$

where the parameter s controls the sparsity. While Achlioptas [68] has proposed the values $s = 1, 2$, Li et al. [69] showed that also very sparse (aggressive) sampling rates like $s = n/\log(n)$ achieve accurate results. Hence, using a modern sparse matrix package allows a rapid execution of (18).

If available, domain specific knowledge can also be utilized to construct the measurement matrix. This allows for more flexibility and makes the approach using compressed sensing interesting and feasible for many domain specific applications.

3.3. GPU Accelerated Implementation

While most current desktop computers allow multithreading and also multiprocessing, using a graphics processing unit (GPU) enables massive parallel processing. The paradigm of parallel computing becomes more important with increasingly large amounts of data and stagnating CPU clock speeds. The architecture of a modern CPU and GPU is illustrated in Figure 3. The key difference between these architectures is that the CPU consists of few arithmetic logic units (ALU) and is highly optimized for low-latency access to cached data sets, while the GPU is optimized for data-parallel, throughput computations. This is achieved by the large number of small arithmetic logic units (ALU).

Traditionally this architecture was designed for the real-time creation of high-definition 2D/3D graphics. However, NVIDIA's programming model for parallel computing *CUDA* opens up the GPU as a general parallel computing device [70]. Using high-performance linear algebra libraries, e.g. *CULA* [71], can help to accelerate comparable CPU implementations substantially. Take for instance the matrix multiplication of two $n \times n$ square matrices, illustrated in Figure 4. The computation involves the evaluation of n^2 dot products.¹ The data parallelism

¹Modern efficient matrix-matrix multiplications are based on block matrix decomposition or other compu-

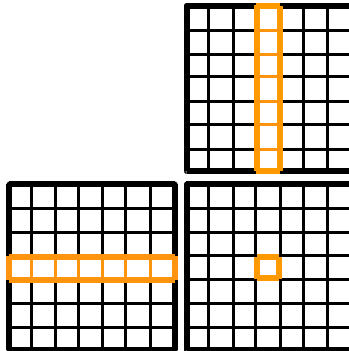


Figure 4: Illustration of the data parallelism in matrix-matrix multiplications.

therein is that each dot-product can be computed independently. With enough ALUs the computational time can be substantially accelerated. This parallelism applies readily to the generation of random numbers and many other linear algebra routines.

Relatively few GPU accelerated background subtraction methods have been proposed so far, for example [72, 73, 74]. The authors achieve considerable speed-ups compared to the corresponding CPU implementations; however, the proposed methods barely exceed 25 frames per second for high definition videos. This is mainly due to the fact that many statistical methods do not fully benefit from the GPU architecture. An advantage of methods based on linear algebra, and hence compressed DMD, is that every operation can benefit from parallel computing. An analysis of Algorithm 1 reveals that generating random numbers in line 3 and the dot products in lines 4, 7, and 9 are particularly suitable for parallel processing. Even when computing the deterministic SVD, the eigenvalue decomposition and the least-square solver benefit from the GPU architecture and are substantially faster than the *MKL* (Intel Math Kernel Library) accelerated routines.

4. Results

In this section we evaluate the computational performance and the suitability of compressed DMD for object detection. To evaluate the detection performance, a foreground mask \mathcal{X} is computed by thresholding the difference between the true frame and the reconstructed background. A standard method is to use the Euclidean distance, leading to the following binary classification problem

$$\mathcal{X}_t(j) = \begin{cases} 1 & \text{if } \|x_{jt} - b_{jt}\| > \tau, \\ 0 & \text{otherwise} \end{cases} \quad (28)$$

where x_{jt} and b_{jt} denote the j -th pixel of the t -th true and background frame. Pixels belonging to foreground objects are set to 1 and 0 otherwise. Access to the true foreground mask allows the computation of several statistical measures. For instance, common evaluation measures in the background subtraction literature [21] are recall, precision and the F-measure. While recall measures the ability to correctly detect pixels belonging to moving objects, precision

tational tricks, and do not actually compute n^2 dot products. However the concept of parallelism remains the same.

measures how many predicted foreground pixels are actually correct, i.e., false alarm rate. The F-measure combines both measures by their harmonic mean. For all computations in the following a standard gaming notebook (Intel Core i7-5500U 2.4GHz, 8GB DDR3 L memory and NVIDIA GeForce GTX 950M) is used.

4.1. Computational performance

First, we compare the computational time and accuracy of compressed DMD using different measurement matrices with randomized DMD [44] and a standard DMD [14] implementation. Therefore, a snapshot sequence with 200 frames is decomposed using $k = 15$ modes. The background is then reconstructed using the first 7 slow varying modes. Figure 5 shows the results for an increasing number of sensors p . The left plot shows the computational speed of the algorithms measured in frames per second (fps). For a small number of sensors all

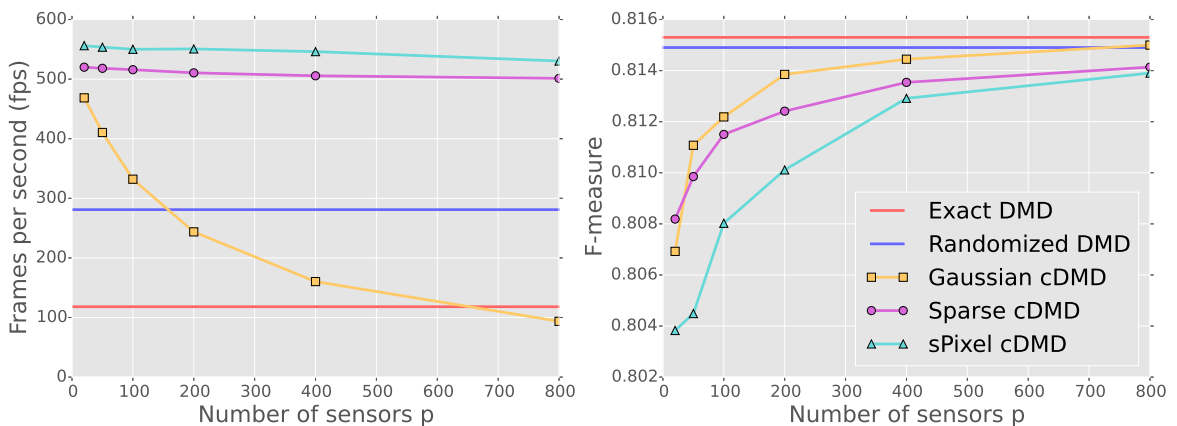


Figure 5: Algorithm runtime with and detection performance against the number of measurements p . Compressed DMD using very sparse or single pixel measurement matrices are about 4-6 times faster than a Gaussian sensing matrix. While single pixel measurements have a higher fps rate, the accuracy is slightly poorer.

three different sensing matrices improve the speed over standard DMD by a factor of about 3 to 5.5. However, for high-dimensional problems involving a large number of sensors, the compression step using a standard Gaussian sensing matrix becomes expensive. Hence, it might not be feasible to use dense random sensing matrices in some applications. Single pixel measurements (sPixel) or the method of very sparse sampling to construct a suitable measurement matrix are more computationally efficient. These techniques come with the cost of a slightly decreased accuracy. The right plot of Fig. 5 shows how the sampling strategies can influence the accuracy in terms of the F-measure. The best convergence rate is achieved using a Gaussian sensing matrix, followed by very sparse sampling. Figure 6 illustrates this further, showing the 3 smallest compressed DMD continuous-time eigenvalues for different numbers of sensors. Most interestingly, the compressed zero mode captures the exact zero mode with high accuracy regardless of the sensing matrix and number of sensors.

This is an important result for background modeling, since the zero mode describes the static background video. The other two modes converge as expected with an increasing number of sensors. Figure 7 shows the F-measure for varying thresholds using just the zero

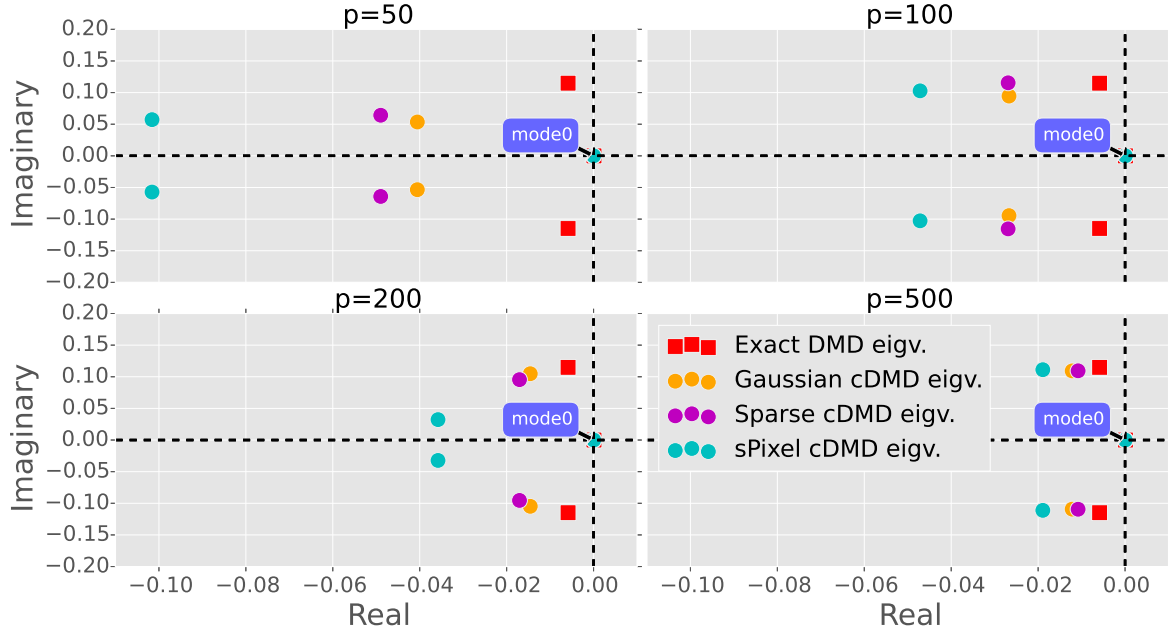


Figure 6: Convergence of compressed DMD continuous-time eigenvalues using different measurement matrices. Using a Gaussian or sparse measurement matrix perform better for small numbers of measurements p . For $p > 500$ the difference to single pixel measurements is negligible.

mode. Sparse and single pixel measurements discard more information than a Gaussian sensing matrix, which can cause a slight loss in accuracy. However, the computation is cheap and hence a large number of sensors can be computed without increasing the computational time significantly. While the use of sparse sensing matrices requires a sparse matrix package which provides algorithms for fast sparse matrix-matrix multiplications, the compression step using single pixel measurements can be implemented readily without the need of any further techniques. Also, using single pixel measurements is the most memory efficient approach. Further, it is important to note that randomized sensing matrices cause random fluctuations, but the variation is relatively small.

Figure 8 shows the average fps rate for different video resolutions. Compressed DMD is capable of processing high definition (HD 720) videos in real-time using smart sensing matrices. For lower resolution videos the fps rate is far above 100. The difference between sPixel and sparse measurement matrices is relatively small. The computational performance of cDMD is achieved by avoiding the expensive computation of the singular value decomposition of the full-state data. The compression step can reduce the time complexity of DMD from $O(knm)$ to $O(kpm)$. However, if full-state DMD modes are required, i.e., the projection of the compressed modes from Φ_Y back to Φ_X , the involved matrix-matrix multiplication requires $O(knm)$. With an increasing video resolution this becomes the computational bottleneck and accounts for the main computational costs. However this computation is also readily parallelizable and a GPU accelerated implementation can substantially improve the computational time. A GPU implementation (here using a Gaussian sensing matrix) can increase the fps rate for HD 1280×720 videos by a factor of about 3, as shown in Figure 8. However, GPU computations require that the data fit into the GPU memory, which is limited

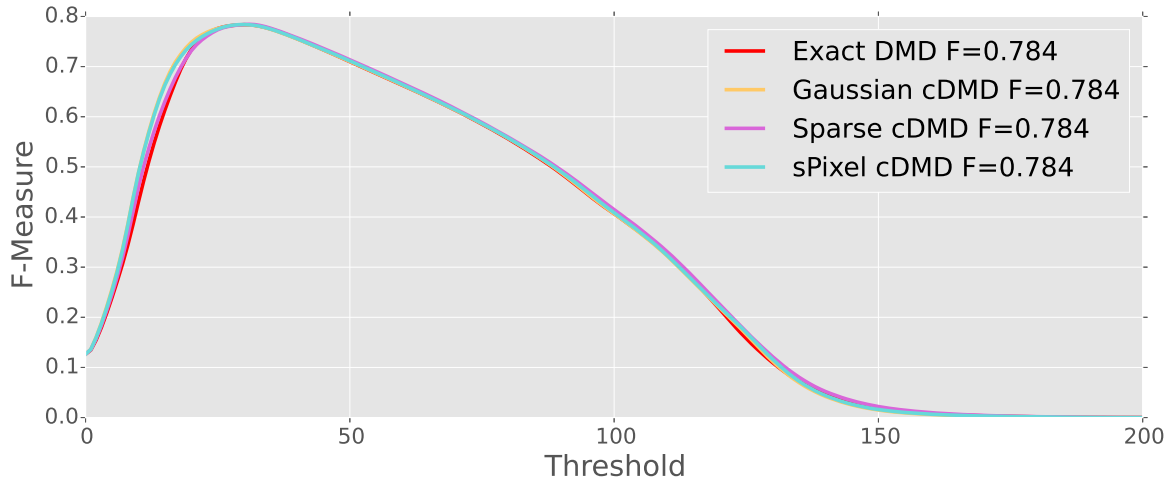


Figure 7: F-measure of varying thresholds measuring the object detection performance of compressed DMD using the zero mode only.

to 8 or 16GB on modern GPUs. Hence, careful and economical data management might be necessary for processing videos beyond full HD quality. Another issue of GPUs is the rather limited bandwidth between CPU and GPU memory. This perceived overhead can be encountered for example using asynchronous memory operations. However, the data transfer should be minimized and good data management depending on the specific problem is necessary.

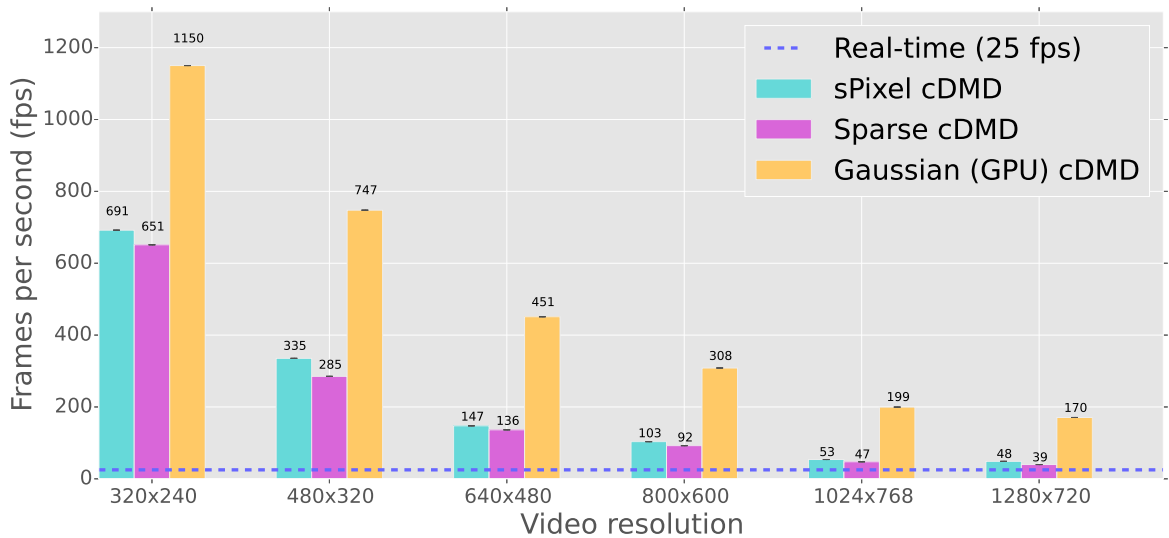


Figure 8: Compressed DMD algorithm runtime on CPU and GPU for videos with different resolutions. The target rank here is fixed to $k = 5$ and the number of sensors to $p = 100$.

4.2. Evaluation on Real Videos

We have evaluated the performance of compressed DMD for object detection using the BMC

(Background Models Challenge) benchmark dataset [75]. Figure 9 illustrates the 9 real videos, posing many common challenges faced in outdoor video surveillance scenarios. Mainly, the



Figure 9: BMC dataset: example frames of the 9 real videos.

following complex situations are encountered:

- **Illumination changes:** Gradual illumination changes caused by fog or sun.
- **Low illumination:** Bad light conditions, e.g., night videos.
- **Bad weather:** Introduced noise (small objects) by weather conditions, e.g., snow or rain.
- **Dynamic backgrounds:** Moving objects belonging to the background, e.g. waving trees or clouds.
- **Sleeping foreground objects:** Former foreground objects that becoming motionless and moving again at a later point in time.

For modeling the background with compressed DMD a low-rank decomposition with target rank $k = 15$ is computed. Moreover, a very sparse measurement matrix with $p = 100$ sensors is used. For the best computational performance we have re-constructed the static background using the zero mode only. Instead, a set of slow varying modes could also be used, allowing slightly better capture of dynamic elements in the background [44]. Some visual results are

presented in Figure 9, showing example frames across 5 videos. The foreground masks show promising results, but some of the raw masks contain small numbers of false positive pixels, however, as shown in the last row of Figure 9 the mask can simply be smoothed using a median filter. For computing the foreground mask an individual threshold value has been selected for each video. The evaluation results computed with the BMC wizard for all 9 videos are shown

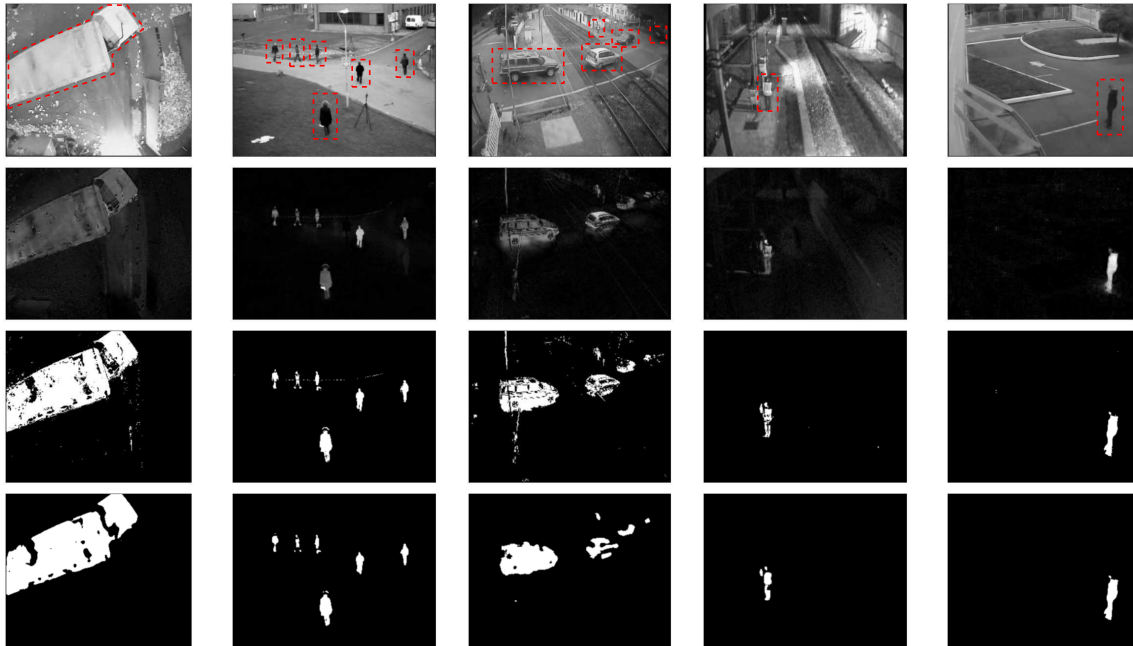


Figure 10: Visual evaluation results for 5 example frames corresponding to the BMC Videos: 002, 003, 006, 007 and 009. The top row is showing the original gray scaled image, where the moving objects are highlighted. The second row is showing the differencing between the reconstructed cDMD background and the original frame. Row three and four are showing the thresholded and median filtered foreground mask.

in Table 1. For comparison we show also the evaluation results [76] of 3 other RPCA methods in addition. Overall cDMD achieves an average F value of about 0.67. This is slightly better than the performance of GoDec [77] and LSADM [78], but it is lower than the F-measure achieved with the RSL method [12]. This indicates that dynamic mode decomposition is a competitive and very fast RPCA approximation. The results also reveal some of the strengths and limitations. Because cDMD is implemented here as a batch algorithm, detecting sleeping foreground objects as they occur in video 001 is difficult. Another weakness is the limited capability of dealing with dynamic and noisy backgrounds, e.g., snow, waving trees and moving clouds as occurring in the videos 001, 005, 008 and 009. On the other hand good results are achieved for the videos 002, 004 and 007, showing that DMD can deal with big moving objects and low illumination conditions. Simple post-processing techniques can further improve the results, in particular the false positive rate caused by dynamic backgrounds can substantially be reduced using a median filter or morphology transformations. Using an adaptive threshold and the integration of compressed DMD into a system allowing background maintenance can lead to further improvements and overcome some of the initial issues.

| Measure | | BMC real videos | | | | | | | | | Average |
|--------------------------------|-----------|-----------------|--------------|--------------|--------------|--------------|-------|--------------|--------------|--------------|---------|
| | | 001 | 002 | 003 | 004 | 005 | 006 | 007 | 008 | 009 | |
| RSL De La Torre et al. [12] | Recall | 0.800 | 0.689 | 0.840 | 0.872 | 0.861 | 0.823 | 0.658 | 0.589 | 0.690 | - |
| | Precision | 0.732 | 0.808 | 0.804 | 0.585 | 0.598 | 0.713 | 0.636 | 0.526 | 0.625 | - |
| | F-Measure | 0.765 | 0.744 | 0.821 | 0.700 | 0.706 | 0.764 | 0.647 | 0.556 | 0.656 | 0.707 |
| LSADM Goldfarb et al. [78] | Recall | 0.693 | 0.535 | 0.784 | 0.721 | 0.643 | 0.656 | 0.449 | 0.621 | 0.701 | - |
| | Precision | 0.511 | 0.724 | 0.802 | 0.729 | 0.475 | 0.655 | 0.693 | 0.633 | 0.809 | - |
| | F-Measure | 0.591 | 0.618 | 0.793 | 0.725 | 0.549 | 0.656 | 0.551 | 0.627 | 0.752 | 0.650 |
| GoDec Zhou and Tao [77] | Recall | 0.684 | 0.552 | 0.761 | 0.709 | 0.621 | 0.670 | 0.465 | 0.598 | 0.700 | - |
| | Precision | 0.444 | 0.682 | 0.808 | 0.728 | 0.462 | 0.636 | 0.626 | 0.601 | 0.747 | - |
| | F-Measure | 0.544 | 0.611 | 0.784 | 0.718 | 0.533 | 0.653 | 0.536 | 0.600 | 0.723 | 0.632 |
| cDMD | Recall | 0.544 | 0.716 | 0.773 | 0.720 | 0.618 | 0.706 | 0.705 | 0.517 | 0.566 | - |
| | Precision | 0.558 | 0.844 | 0.815 | 0.781 | 0.576 | 0.736 | 0.825 | 0.529 | 0.577 | - |
| | F-Measure | 0.551 | 0.775 | 0.794 | 0.750 | 0.596 | 0.720 | 0.760 | 0.523 | 0.571 | 0.671 |

Table 1: Evaluation results of nine real videos from the BMC dataset. For comparison, the results of three other leading robust PCA algorithms are presented, adapted from [76].

5. Conclusion and Outlook

We have introduced compressive dynamic mode decomposition as a novel algorithm for foreground/background separation of video content. Although many techniques have been developed in the last decade and a half to accomplish this task, significant challenges remain for the computer vision community when real-time processing of high-definition video is required. Indeed, real-time HD video analysis remains one of the grand challenges of the field. Our cDMD method provides compelling evidence that it is a viable candidate for meeting this grand challenge, even on standard CPU computing platforms. On a GPU architecture, the method is well above the required real-time processing rate, thus allowing for a host of other algorithms to be applied to the foreground video that may be of critical use such as object identification and tracking.

The cDMD method also allows us to potentially reframe the real-time HD challenge. Specifically, it is not enough simply to execute the foreground/background subtraction in real-time. Rather, one would like to enact this process with substantial computational time to spare so that a host of other potential computer vision algorithms can be enacted to analyze the video. For instance, one may execute face detection algorithms, object detection subroutines, etc. Given the computational margin gained, one can also improve the quality of the foreground/background subtraction, as measured by the F-measure, with additional algorithms. Each additional algorithm has a prescribed computational overhead. Thus in order to keep a computer vision algorithm running in real time, the foreground/background separation portion must occur well below real-time processing. As such, cDMD is demonstrated here to be a viable candidate even under this more stringent processing time requirement.

Despite the significant computational savings, the cDMD remains competitive with other leading algorithms in the quality of the decomposition itself. Future work will aim to improve the overall quality of background/foreground separation as well as to integrate a number of innovative techniques. One technique that is particularly useful for object tracking is the multi-resolution DMD [37]. This algorithm has been shown to be a potential method for target tracking applications. Thus one can envision the integration of multi-resolution ideas with cDMD, i.e. a multi-resolution compressive DMD (mrcDMD) method, in order to separate the foreground video into different dynamic targets when necessary.

Acknowledgements

JNK acknowledges support from Air Force Office of Scientific Research (FA9500-15-C-0039). SLB acknowledges support from the Department of Energy under award DE-EE0006785. NBE acknowledges support from the UK Engineering and Physical Sciences Research Council.

References

- [1] J. Grosek, J. N. Kutz, Dynamic mode decomposition for real-time background/foreground separation in video (2014). [arXiv:1404.7592](https://arxiv.org/abs/1404.7592).
- [2] S. Brunton, J. Proctor, J. N. Kutz, *Compressive sampling and dynamic mode decomposition*, Journal of Computational Dynamics.
- [3] C. Stauffer, W. Grimson, *Adaptive background mixture models for real-time tracking*, Proceedings IEEE Conf. on Computer Vision and Pattern Recognition, 1999.
- [4] K. Toyama, J. Krumm, B. Brumitt, B. M. B, *Wallflower: principles and practice of background maintenance*, Proceedings of the Seventh IEEE International Conference on Computer, 1999.
- [5] L. Cheng, M. Gong, *Realtime Background Subtraction from Dynamic Scenes*, International Conference on Computer Vision, 2009.
- [6] L. Li, W. Huang, I. Gu, Q. Tian, *Statistical Modeling of Complex Backgrounds for Foreground Object Detection*, IEEE Transactions on Image Processing 13 (11) (2004) 1459–1472.
- [7] N. Oliver, B. Rosario, A. Pentland, *A Bayesian computer vision system for modeling human interactions*, ICVS.
- [8] Y. Tian, M. Lu, A. Hampapur, *Robust and Efficient Foreground Analysis for Real-Time Video Surveillance*, in: IEEE Computer Society Conference on Computer Vision and Pattern Recognition, 2005., Vol. 1, 2005, pp. 1182–1187.
- [9] L. Maddalena, A. Petrosino, *A Self-Organizing Approach to Background Subtraction for Visual Surveillance Applications*, IEEE Transactions on Image Processing 17 (7) (2008) 1168–1177.
- [10] J. He, L. Balzano, A. Szlam, *Incremental Gradient on the Grassmannian for Online Foreground and Background Separation in Subsampled Video*, in: Computer Vision and Pattern Recognition (CVPR), 2012 IEEE Conference on, 2012, pp. 1568–1575.
- [11] E. Candès, X. Li, Y. Ma, J. Wright, *Robust Principal Component Analysis?*, Computing Research Repository abs/0912.3599.
- [12] F. D. la Torre, M. Black, *A Framework for Robust Subspace Learning*, International Journal of Computer Vision 54 (1-3) (2003) 117–142.
- [13] P. Huber, *Robust Statistics*, Wiley, 1981.

- [14] J. N. Kutz, J. Grosek, S. L. Brunton, Dynamic mode decomposition for robust pca with applications to foreground/background subtraction in video streams and multi-resolution analysis, in *CRC Handbook on Robust Low-Rank and Sparse Matrix Decomposition: Applications in Image and Video Processing*, T. Bouwmans Ed.
- [15] J. N. Kutz, J. Grosek, S. L. Brunton, Multi-resolution time-scale separation of video content using the dynamic mode decomposition, *Proceeding of the Ninth International Workshop on Video Processing and Quality Metric for Consumer Electronics, VPQM 2015*, paper 14, Chandler, AZ.
- [16] Y. Benezeth, P.-M. Jodoin, B. Emile, H. Laurent, C. Rosenberger, *Comparative Study of Background Subtraction Algorithms*, *Journal of Electronic Imaging* 19 (2010) 19 (3) (2010) 033003.
- [17] T. Bouwmans, *Recent advanced statistical background modeling for foreground detection: a systematic survey*, *RPCS* 4(3) (2011) 147–176.
- [18] M. Shah, J. Deng, B. Woodford, *Video Background Modeling: Recent Approaches, Issues and Our Solutions*, *Machine Vision and Applications, Special Issue on Background Modeling for Foreground Detection in Real-World Dynamics* 25 (2014) 1105–1119.
- [19] A. Shimada, D. Arita, R. Taniguchi, *Dynamic control of adaptive mixture of Gaussians background model*, 2006.
- [20] T. Bouwmans, E. H. Zahzah, *Robust PCA via Principal Component Pursuit: A review for a comparative evaluation in video surveillance*, *Comp. Vis. Imag. Under.* 122 (2014) 22–34.
- [21] E. T. Bouwmans, *Handbook on Robust Decomposition in Low Rank and Sparse Matrices and its Applications in Image and Video Processing*, CRC Press, 2015.
- [22] T. Bouwmans, [Background subtraction website](https://sites.google.com/site/backgroundsubtraction/Home) (2015).
URL <https://sites.google.com/site/backgroundsubtraction/Home>
- [23] M. Kleinsteuber, F. Seidel, C. Hage, *pROST: A Smoothed ℓ_p -Norm Robust Online Subspace Tracking Method for Realtime Background Subtraction in Video*, *Machine Vision and Applications, Special Issue on Background Modeling for Foreground Detection in Real-World Dynamic Scenes*.
- [24] C. Hage, M. Kleinsteuber, *Robust PCA and Subspace Traking from incomplete Observations Using ℓ_0 -Surrogates* (2013). [arXiv:1210.0805v2](https://arxiv.org/abs/1210.0805v2).
- [25] P. Schmid, *Dynamic mode decomposition of numerical and experimental data*, *Journal of Fluid Mechanics* 656 (2010) 5–28.
- [26] C. Rowley, I. Mezić, S. Bagheri, P. Schlatter, D. Henningson, *Spectral analysis of non-linear flows*, *Journal of Fluid Mechanics* 641 (2009) 115–127.
- [27] J. Tu, C. Rowley, D. Luchtenberg, S. Brunton, J. N. Kutz, *On Dynamic Mode Decomposition: Theory and Applications*, *Journal of Computational Dynamics* 1 (2014) 391–421.

- [28] J. N. Kutz, *Data-driven modeling and scientific computing: Methods for Integrating Dynamics of Complex Systems and Big Data*, Oxford Press, 2013.
- [29] K. Chen, J. Tu, C. Rowley, *Variants of Dynamic Mode Decomposition: Boundary Condition, Koopman, and Fourier Analyses*, *Journal of Nonlinear Science* 22 (6) (2012) 887–915.
- [30] B. Koopman, Hamiltonian systems and transformation in hilbert space, *Proc. Nat. Acad. Sci.* 17 (1931) 315–318.
- [31] I. Mezić, A. Banaszuk, Comparison of systems with complex behavior, *Physica D: Nonlinear Phenomena* 197 (2004) 101 – 133.
- [32] I. Mezić, *Analysis of Fluid Flows via Spectral Properties of the Koopman Operator*, *Annual Review of Fluid Mechanics* 45 (2013) 357–378.
- [33] J. N. Kutz, S. L. Brunton, B. Brunton, J. L. Proctor, Dynamic mode decomposition: Applications of equation-free modeling to complex systems, *SIAM* (to appear).
- [34] M. R. Jovanović, P. J. Schmid, J. W. Nichols, Sparsity-promoting dynamic mode decomposition, *Physics of Fluids* 26 (2) (2014) 024103.
- [35] J. H. Tu, C. W. Rowley, J. N. Kutz, J. K. Shang, Spectral analysis of fluid flows using sub-Nyquist rate PIV data, *Experiments in Fluids* 55 (9) (2014) 1–13.
- [36] F. Gueniat, L. Mathelin, L. Pastur, A dynamic mode decomposition approach for large and arbitrarily sampled systems, *Physics of Fluids* 27 (2) (2015) 025113.
- [37] J. N. Kutz, X. Fu, S. L. Brunton, Multi-resolution dynamic mode decomposition, *SIAM J. App. Dyn. Sys.* (to appear).
- [38] J. Proctor, S. Brunton, J. N. Kutz, *Dynamic mode decomposition with control*, arXiv:1409.6358.
- [39] S. Dawson, M. Hemati, M. Williams, C. Rowley, Characterizing and correcting for the effect of sensor noise in the dynamic mode decomposition, *Bulletin of the American Physical Society* 59.
- [40] M. S. Hemati, C. W. Rowley, De-biasing the dynamic mode decomposition for applied koopman spectral analysis (2015). [arXiv:1502.03854](https://arxiv.org/abs/1502.03854).
- [41] B. Brunton, L. Johnson, J. Ojemann, J. N. Kutz, Extracting spatial-temporal coherent patterns in large-scale neural recordings using dynamic mode decomposition, *J. Neuroscience Methods* (to appear).
- [42] J. Proctor, P. Echhoff, Discovering dynamic patterns from infectious disease data using dynamic mode decomposition, *International Health* 7 (2015) 139–145.
- [43] E. Berger, M. Sastuba, D. Vogt, B. Jung, H. B. Amor, Dynamic mode decomposition for perturbation estimation in human robot interaction, in: *23rd IEEE International Symposium on Robot and Human Interactive Communication*, 2014.

- [44] N. B. Erichson, C. Donovan, Randomized low-rank dynamic mode decomposition for motion detection (2015). [arXiv:1512.03526](#).
- [45] L. N. Trefethen, D. Bau, *Numerical Linear Algebra*, SIAM, Philadelphia, 1997.
- [46] M. Gavish, D. Donoho, The optimal hard threshold for singular values is $4/\sqrt{3}$, *Information Theory, IEEE Transactions on* 60 (8) (2014) 5040–5053. [doi:10.1109/TIT.2014.2323359](#).
- [47] D. L. Donoho, Compressed sensing, *IEEE Transactions on Information Theory* 52 (4) (2006) 1289–1306.
- [48] E. J. Candès, J. Romberg, T. Tao, Robust uncertainty principles: exact signal reconstruction from highly incomplete frequency information, *IEEE Transactions on Information Theory* 52 (2) (2006) 489–509.
- [49] E. J. Candès, T. Tao, Near optimal signal recovery from random projections: Universal encoding strategies?, *IEEE Transactions on Information Theory* 52 (12) (2006) 5406–5425.
- [50] E. J. Candès, J. Romberg, T. Tao, Stable signal recovery from incomplete and inaccurate measurements, *Communications in Pure and Applied Mathematics* 8 (1207–1223).
- [51] R. G. Baraniuk, Compressive sensing, *IEEE Signal Processing Magazine* 24 (4) (2007) 118–120.
- [52] R. G. Baraniuk, V. Cevher, M. F. Duarte, C. Hegde, Model-based compressive sensing, *IEEE Transactions on Information Theory* 56 (4) (2010) 1982–2001.
- [53] E. J. Candès, M. B. Wakin, An introduction to compressive sampling, *IEEE Signal Processing Magazine* (2008) 21–30.
- [54] E. J. Candès, Compressive sensing, *Proceedings of the International Congress of Mathematics*.
- [55] A. C. Gilbert, P. Indyk, Sparse recovery using sparse matrices, *Proceedings of the IEEE* 98 (6) (2010) 937–947.
- [56] I. Bright, G. Lin, J. N. Kutz, Compressive sensing and machine learning strategies for characterizing the flow around a cylinder with limited pressure measurements, *Physics of Fluids* 25 (2013) 127102–1–127102–15.
- [57] Z. Bai, T. Wimalajeewa, Z. Berger, G. Wang, M. Glauser, P. K. Varshney, Physics based compressive sensing approach applied to airfoil data collection and analysis, *AIAA Paper 2013-0772*, 51st Aerospace Sciences Meeting (January 2013).
- [58] Z. Bai, T. Wimalajeewa, Z. Berger, G. Wang, M. Glauser, P. K. Varshney, Low-dimensional approach for reconstruction of airfoil data via compressive sensing, *AIAA Journal* (2014) 1–14.
- [59] B. W. Brunton, S. L. Brunton, J. L. Proctor, J. N. Kutz, Optimal sensor placement and enhanced sparsity for classification, submitted for publication.

- [60] J. A. Tropp, Greed is good: Algorithmic results for sparse approximation, *IEEE Transactions on Information Theory* 50 (10) (2004) 2231–2242.
- [61] J. A. Tropp, J. N. Laska, M. F. Duarte, J. K. Romberg, R. G. Baraniuk, Beyond Nyquist: Efficient sampling of sparse bandlimited signals, *IEEE Transactions on Information Theory* 56 (1) (2010) 520–544.
- [62] D. Needell, J. A. Tropp, CoSaMP: iterative signal recovery from incomplete and inaccurate samples, *Communications of the ACM* 53 (12) (2010) 93–100.
- [63] A. C. Gilbert, J. Y. Park, M. B. Wakin, Sketched SVD: Recovering spectral features from compressive measurements, *ArXiv e-prints*.
- [64] W. B. Johnson, J. Lindenstrauss, Extensions of lipschitz mappings into a hilbert space, *Contemporary mathematics* 26 (189-206) (1984) 1.
- [65] J. E. Fowler, Compressive-projection principal component analysis, *IEEE Transactions on Image Processing* 18 (10) (2009) 2230–2242.
- [66] H. Qi, S. M. Hughes, Invariance of principal components under low-dimensional random projection of the data, *IEEE International Conference on Image Processing (October 2012)*.
- [67] F. Woolfe, E. Liberty, V. Rokhlin, M. Tygert, A fast randomized algorithm for the approximation of matrices, *Applied and Computational Harmonic Analysis* 25 (3) (2008) 335–366.
- [68] D. Achlioptas, Database-friendly random projections: Johnson-lindenstrauss with binary coins, *Journal of computer and System Sciences* 66 (4) (2003) 671–687.
- [69] P. Li, T. J. Hastie, K. W. Church, Very sparse random projections, in: *Proceedings of the 12th ACM SIGKDD international conference on Knowledge discovery and data mining*, ACM, 2006, pp. 287–296.
- [70] J. Nickolls, I. Buck, M. Garland, K. Skadron, Scalable parallel programming with cuda, *Queue* 6 (2) (2008) 40–53. doi:10.1145/1365490.1365500.
- [71] J. R. Humphrey, D. K. Price, K. E. Spagnoli, A. L. Paolini, E. J. Kelmelis, Cula: hybrid gpu accelerated linear algebra routines (2010). doi:10.1117/12.850538.
- [72] P. Carr, Gpu accelerated multimodal background subtraction, in: *Digital Image Computing: Techniques and Applications*, IEEE, 2008, pp. 279–286.
- [73] V. Pham, P. Vo, V. T. Hung, et al., Gpu implementation of extended gaussian mixture model for background subtraction, in: *Computing and Communication Technologies, Research, Innovation, and Vision for the Future (RIVF)*, 2010 IEEE RIVF International Conference on, IEEE, 2010, pp. 1–4.
- [74] Q. Lixia, S. Bin, L. Weiyao, W. Wen, S. Ruimin, Gpu-accelerated video background subtraction using gabor detector, *Journal of Visual Communication and Image Representation* 32 (2015) 1 – 9. doi:10.1016/j.jvcir.2015.07.010.

- [75] A. Vacavant, T. Chateau, A. Wilhelm, L. Lequievre, A benchmark dataset for outdoor foreground/background extraction, in: *Computer Vision–ACCV 2012 Workshops*, Springer, 2013, pp. 291–300.
- [76] T. Bouwmans, A. Sobral, S. Javed, S. K. Jung, E.-H. Zahzah, Decomposition into low-rank plus additive matrices for background/foreground separation: A review for a comparative evaluation with a large-scale dataset (2015). [arXiv:1511.01245](https://arxiv.org/abs/1511.01245).
- [77] T. Zhou, D. Tao, Godec: Randomized low-rank & sparse matrix decomposition in noisy case, in: *International Conference on Machine Learning, ICML, 2011*, pp. 1–8.
- [78] D. Goldfarb, S. Ma, K. Scheinberg, Fast alternating linearization methods for minimizing the sum of two convex functions, *Mathematical Programming* 141 (1-2) (2013) 349–382. [doi:10.1007/s10107-012-0530-2](https://doi.org/10.1007/s10107-012-0530-2).

Affiliation:

N. Benjamin Erichson
School of Mathematics and Statistics
University of St Andrews
KY16 9LZ St Andrews, United Kingdom
E-mail: nbe@st-andrews.ac.uk

Steven L. Brunton
Department of Mechanical Engineering
University of Washington
Seattle, WA 98195

J. Nathan Kutz
Department of Applied Mathematics
University of Washington
Seattle, WA 98195-2420